Label-Free Perfect Separation of Michigan Cancer Foundation-7 Cells from White Blood Cells using Both Wall-Induced Lift and Dielectrophoresis Forces

Alireza Alaghemand
Electrical Engineering Department, Shahrood University of Technology, Shahrood, Iran
E-mail: alireza.alaghemand@shahroodut.ac.ir

Ali Fattah *
Electrical Engineering Department, Shahrood University of Technology, Shahrood, Iran
E-mail: a.fattah@shahroodut.ac.ir
*Corresponding author

Received: 23 April 2022, Revised: 2 August 2022, Accepted: 7 August 2022

Abstract: A microchannel device was designed and utilized to separate Michigan Cancer Foundation-7 cells from white blood cells using both wall-induced lift and di-electrophoresis forces. Using COMSOL Multiphysics simulator, the label-free separation process is performed based on the radius size of the particles. The best performance of the structure is obtained with the efficiency of 100% and 99% for cancer and white blood cells separation processes, respectively. For the proposed microfluidic structure, in addition to the highest available efficiency and high separation speed of 12 um/s, the low DC voltage of 6 V is applied, which causes negligible damage to the blood cells.

Keywords: Cancer Cells, COMSOL, Dielectrophoresis, Microfluidics, Separation

How to cite this paper: Alireza Alaghemand, and Ali Fattah, "Label-Free Perfect Separation of Michigan Cancer Foundation-7 Cells from White Blood Cells using Both Wall-Induced Lift and Dielectrophoresis Forces", Int J of Advanced Design and Manufacturing Technology, Vol. 15/No. 3, 2022, pp. 99-107.
DOI: 10.30486/admt.2022.1957227.1347.

Biographical notes: Alireza Alaghemand received his BSc in Electrical Engineering from Tehran Azad University, South Tehran Branch, and his MSc from Shahrood University of Technology, in 2017 and 2021, respectively. His current research interest includes Microfluidic and Nanofluidic structures. **Ali Fattah** is an Assistant Professor of Electronic Engineering at Shahrood University of Technology, Iran. He received his PhD in Electronic Engineering from Amirkabir University of Technology, in 2014. His current research focuses on Organic Electronics, Photovoltaics and Detection and Separation processes using Microfluidic devices.

1 INTRODUCTION

Microfluidic is defined as the science and technology of device analysis that works with fluids in very small sizes. This technology which uses channels with dimensions of several tens to a few hundred micrometers, has many applications in various sciences, from chemical synthesis and biological analysis to optics and information technology [1]. Microfluidic was used in laboratory because of its unique properties including the ability to perform measurements with a small amount of sample, separations with high accuracy and sensitivity, low cost and short time to perform assays [2]. One of the most widely used methods in the field of isolation and manipulation of biological cells is dielectrophoresis. The directional motion of neutral particles in an uneven electric field is called dielectrophoresis [3], which is widely used in specialized medical and research laboratories for diagnosis, treatment of diseases and research on cells. Cancer cells are electrically neutral but as are exposed to an uneven electric field, they become electrically polarized and will move in the opposite direction of the field under the influence of the electric field [4-5].

Although it is widely accepted that early detection is the only definitive way to defeat cancer, today in most developed countries, cancer diagnosis relies on expensive imaging instruments. Although the Circulation of Tumor Cell (CTC) is an important marker for different types of cancer, they are so rare in the bloodstream and their accurate analysis and isolation is a challenging task [6-7]. Pommer et al. designed a two-stage microfluidic device to separate platelets from whole blood samples. This device used a relatively high voltage difference of 100 volts at a frequency of 1 MHz to separate the desired particles [8]. Han and Frazier developed a dielectrophoresis device for separating White Blood Cells (WBCs) from Red Blood Cells (RBCs) using two different geometric designs of the device to compare the rate of separation of the cells [9]. In [10], isolation is done based on frequency changes using a device that isolate the red blood cells from the infected ones as a pathogen. The operation of the device is based on the electrode's location next to the channel wall and creation of an electric field at different frequencies which separates particles upon the force of dielectrophoresis. Park et al. investigated the effects of buffer input velocity on cell separation efficiency in a microfluidic apparatus using adsorption forces and dielectric repulsion. They concluded that as the buffer rate increases, the separation efficiency decreases [11]. A microfluidic device based on flow field refraction for separation of platelets from whole blood is designed where a small applied voltage yields to a high separation rate [12]. Patel et al. developed a device for separating dead cells from living ones using dielectrophoresis method where separation operation is performed with an electric field variation [13]. It has been shown that electric field buffer velocity and channel width are considered as the important parameters of the separation. A simple microfluidic design for separation of the particles with dimensions of 30 nm and 60 nm has been presented, where the improvement of the separation efficiency is done by changing the buffer speed [14]. Kiel et al. introduced a microfluidic device based on dielectrophoresis to separate particles with a diameter of 5μm which examines the result of separation by applying different voltages, but due to the usage of alternating voltage, a high voltage value was needed [15]. A microfluidic device is proposed which creates a non-uniform flow by creating teeth gratings in the main channel to separate different types of cancer cells [16].

As is reviewed, most of the previous studies have focused on the isolation of white blood platelets and globules from the whole blood, and the isolation of cancer cells has been less considered. The difference in radius size and permeability coefficient of the cancer cells compared to the other components of the blood can significantly affect the isolation yield. As the Michigan Cancer Foundation-7 (MCF-7) cells and WBCs overlap in size, their separation is difficult. To perform a perfect separation, the combination of di-electrophoresis and wall-induced lift force is used here. To achieve this goal, the channel dimensions and applied voltage on the electrodes are calculated. Using the designed square structures, the combination of the cells tends to create a non-uniform buffer flow and as the particles are affected by the wall-induced lift force, they enter the main channel. As the applied voltage to the electrodes creates a non-uniform electric field, the separation takes place by the effect of both wall-induced lift and dielectrophoresis forces. Compared to previously published investigations, it tends to not only the highest label-free separation efficiency and a high separation speed, but also to a low voltage application, which causes less damage to the blood cells.

2 SEPARATION MECHANISM AND STRUCTURE DESIGN

2.1. Theory Description

In the present study, both the wall-induced lift and di-electrophoresis effects are applied to perform the separation process. More detailed, these effects can be divided into three forces of Wall-induced lift, Drag and Dielectrophoresis, which will be described in this section.

All gases and many liquids can be considered Newtonian. Examples of non-Newtonian fluids are honey, mud, blood, liquid metals, and most polymer solutions [17]. The existence of square structures creates

a velocity gradient of fluid and possibly causes the rotation of spherical particles. Therefore, wall-induced lift force may act on the cells to move the cells laterally. The mechanism of wall-induced lift force for the cell moving parallel to a wall in the fluid is as follows. The vorticity caused around the cell diffuses downstream and interacts with the wall, and this interaction results in a net lift force on the cell-directed away from the wall [18].

First, we consider the case where the dimension of cells is smaller than that of the channel. The cells are mostly affected by a single wall where the direction of the particle motion can be parallel to the walls. A first-order correction factor for the drag coefficient of a small cell in the creeping flow moving towards a solid wall is derived [19]. The wall-induced lift force (F_w) can be calculated as follows:

$$f_w = \frac{16\mu v}{a}k \tag{1}$$

Where, μ, v and a are the fluid viscosity, the fluid velocity, and the cell diameter, respectively. The k is the hydrodynamic force on the particle which is calculated as follow:

$$k = \sinh\theta \sum_{n=1} \frac{n(n+1)}{(2n-1)(2n+3)} \times \left[\frac{2\sinh(2n+1)\theta + (2n+1)\sinh 2\theta}{4\sinh^2(0.5+n)\theta - (2n+1)^2 \sinh^2 2\theta} - 1 \right] \tag{2}$$

Where, θ is a function of the ratio of the distance from the sphere center to the wall to the particle diameter. Considering Equation (2), as a particle approaches a wall, the hydrodynamic force is increased. In addition to the force of wall-induced lift, another force called the Drag force acts on the cells, which its amount depends on the speed difference between the fluid and the blood cell suspended in. As a small cell is moving in a fluid medium at the velocity of v, the particle would expose to a resistive force from the fluid with the viscosity which is called the drag force, and can be obtained as follow [20]:

$$F_{Drag} = \frac{1}{2}cA\rho v^2 \tag{3}$$

Where, c, A and ρ are the Drag coefficient, the area of the object and the density of the fluid, respectively. Figure 1 shows inertial forces importing on the particle.

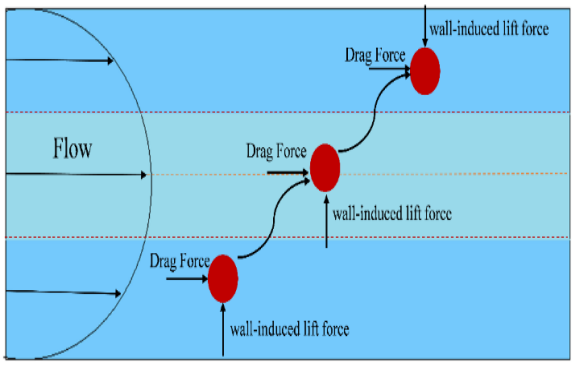

Fig. 1 Drag and lift forces on solid spherical particles in wall-bounded flows.

Dielectrophoresis is a force that affects the motion of particles and its amount depends on the difference between the permeability coefficients of the cell and the fluid around it. The dielectric force applied to a neutral spherical particle which is polarizable and located in a conductive medium is obtained as the following Equation [21]:

$$f_{DEP} = 2\pi r^3 \varepsilon_m R_e\left[f_{cm}\right]\nabla E^2 \tag{4}$$

Where, r is the particle radius, ε_m is particle permeability, ∇E is the electrical field intensity and $R_e[f_{cm}]$ is the real part of Clausius-Mossotti factor obtained as $f_{cm} = (\varepsilon_{eq} - \varepsilon_m)/(\varepsilon_{eq} + 2\varepsilon_m)$, where ε_m is the permeability coefficient for the medium and ε_{eq} is the complex permeability coefficient. In this study, the single-shell model feature is used to calculate the dielectric forces exerted on cells because considering the outer layer of the cells, this model provides an accurate estimation of ε_{eq} which is calculated based on the following Equation:

$$\varepsilon_{eq} = \frac{d^3 + 2\left(\frac{\varepsilon_n - \varepsilon_s}{\varepsilon_n + 2\varepsilon_s}\right)}{d^3 - \left(\frac{\varepsilon_n - \varepsilon_s}{\varepsilon_n + 2\varepsilon_s}\right)} \tag{5}$$

In which, ε_n and ε_s are the cytoplasm and the membrane permeability coefficients, respectively. Moreover, the d value is obtained from d=ro/ri where r_o and r_i denote the inner and outer radiuses of the cell, respectively. Also, "Fig. 2" depicts the single-shell model of the cell. The physical and dielectric properties and also the related parameters of the cell are listed in "Table 1", where σ_n and σ_s are the conductivity coefficients and ε_n and ε_s are the permeability of the cytoplasm and membrane layers of the cell, respectively [22-23].

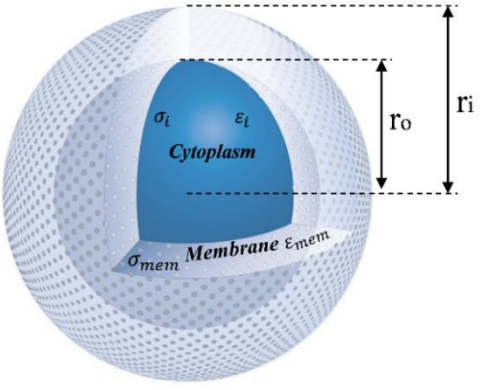

Fig. 2 Single-shell model of the cell.

Table 1 Dielectric properties of cells

Property	Unit	WBC	MCF-7
r_i	mμ	12	12
r_o	mμ	7	1
σ_n	S/m	0/65	0/8
ε_n	–	60	60
σ_s	S/m	0/00027	0/00015
ε_s	–	6	6

Considering the electric field application, the dielectrophoresis force acting on the particles will be different which causes the particles to move. Depending on the polarizability of the particles, compared with that of the medium, the force would push the particles towards the regions with higher or lower potential.
Furthermore, if the particles have a higher polarizability (conductivity) than their immersion medium, they move toward regions with high electric field. Conversely, if the particles have lower conductivity than their medium, they move away from regions with high electric field toward the regions with low electric field. The movement of the particle toward a high electric field region is called positive dielectrophoresis (+DEP), while its movement toward a low electric field region is called negative dielectrophoresis (−DEP) [24].

2.2. Structure Design

There are quite a few designs that use wall-induced lift force to separate cancer cells from the Blood-forming particles [25]. Our proposed microfluidic device consists of an array of square structures connected to the main channel. These expansion-contraction arrays cause the inertial motion, as without the existence of the arrays, the fluid flow will be uniform and there would be no velocity gradient and therefore no lateral lift force appears. CTCs are affected by the inertial lift force, moving towards the contraction-expansion flow side, while WBCs are influenced by the Drag force, moving towards the opposite side [26]. But, as the CTCs and WBCs have almost similar size, their perfect separation using only wall-induced lift force is difficult [27-28]. To perform a full separation, dielectrophoresis force is then generated using electrodes placed at the channel wall. Therefore, separating process is performed based on the characterization of cellular and membrane capacitance [29].
Figure 3 depicts the designed structure of the microfluidic, where both the WBCs and CTCs enter the main channel simultaneously and the buffer fluid enters from the other input. Considering the fabrication process limitations, the width of the main channel and the square structures sections are selected as W = 20um and W = 25um, respectively. The DC voltages are applied to an array of electrodes placed at the channel wall. Considering the location of electrodes, CTCs and WBCs are exposed to DEP force in the y-direction. It turns out that to create a non-uniform electric field, the applied voltage must be 6 volts. This voltage is selected to separate CTCs and to preserve cell viability for perfect analysis.

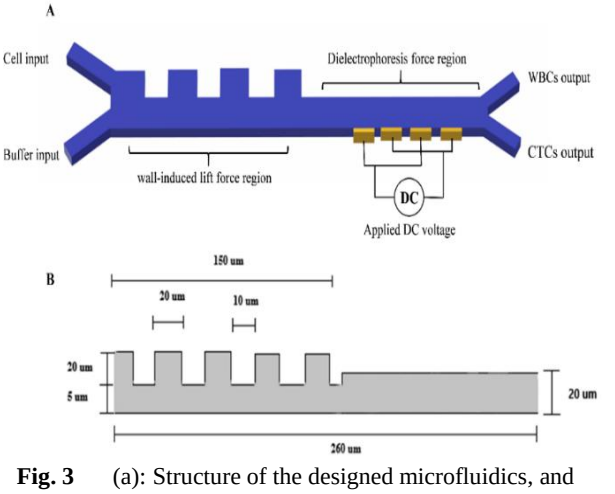

Fig. 3 (a): Structure of the designed microfluidics, and (b): Channel dimensions.

Fluid velocity is one of the most influential factors in the separation efficiency, as if the velocity be low, it will cause more particles to be affected by the non-uniform electric field and further deflect towards the electrodes, which causes them to stick to the electrodes. Otherwise, if the fluid velocity be too high, it yields to the micro-channel blockage. Equation Q=V.A is used to obtain the proper fluid velocity, where Q is the flow rate, A is the micro-channel cross section area and V is the fluid velocity. On the other hand, the width of the channel must be chosen so the created electric field covers it all. Employing Q=V.A, the ratio of fluid velocity to channel width is obtained as “Fig. 4”. In the section of square structures, due to its less cross section area, the instantaneous flow rate is higher than the main channel.

Therefore, the rate of cell transport in square structures is higher.

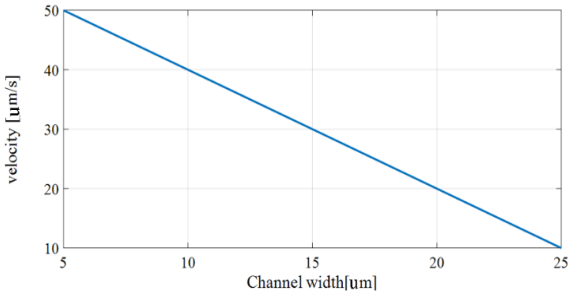

Fig. 4 Velocity profile in terms of the channel width.

The electric field intensity as another effective factor on separation efficiency, is proportional to the applied voltage and the inverse of distance between the electrodes. Using Equation $E=V_{ab}/\ d$, the distance between the electrodes and the appropriate voltage to create the required electric field are determined. Considering "Fig. 5", the distance between the electrodes is selected as d = 3 um. Due to the incompressibility of the fluid, it can be concluded that the rate of input flow is equal to the output, so the flow rate of Q = 2.7×10E-14 m^3/S and the intensity of electric field of E = 2×10E6 V/m in the main channel are obtained. These values are well compatible with [12]. The particles enter the square structures at a speed of 12um/s while they are affected by Drag force of 0.027N. Next, the particles enter the main channel and are separated by a dielectric force of 0.15N based on the size of the particle.

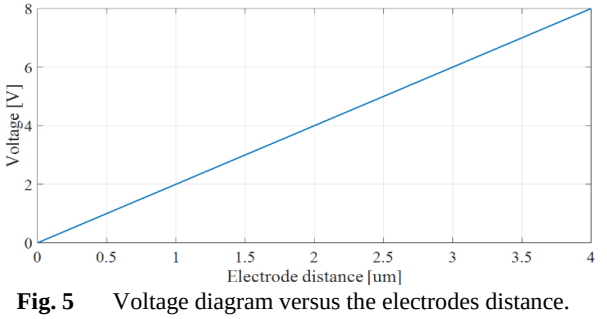

Fig. 5 Voltage diagram versus the electrodes distance.

The selected dimensions of the channel which is made of PDMS, according to the design process are 300um by 20um. Also, the fluid specifications are given in "Table 2".

Table 2 Buffer fluid specifications

Property	Unit	Value
Density	kg/m^3	1000
Viscosity	Pa × s	100
Conductivity	Farad/Meter	78
Permeability	/m)Ʊ(Siemens	210
Temperature	K	273

3 RESULTS AND DISCUSSION

The simulations are performed using COMSOL Multiphysics as a cross-platform finite element analysis to isolate the MCF-7 cells from the WBCs. In the case of discretization, we mean breaking the geometry into smaller and discrete parts. This occurs by dividing the geometry into several smaller and separate units called elements, and the solution is obtained by pasting low-order polynomials into each element to form a single function. There are two basic factors to consider in discretization. First, how to divide geometry. The second is how to resolve between nodes. Doing the mesh of the geometry in our model, we are able to do it either automatically or manually. In our simulations, due to the simplicity of the structure, we have used the automatic one. Considering "Fig. 6", the mesh size for the square part is 3 nm while for the rest part of the channel with a simpler structure, the mesh size is 6 nm.

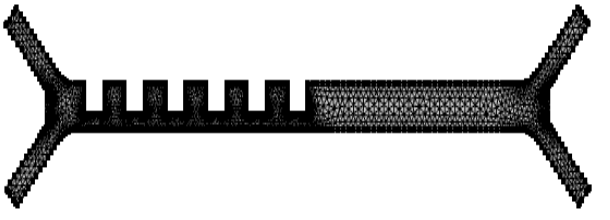

Fig. 6 Meshing of the structure.

3.1. Electric Field Distribution

Figure 7 shows the distribution of the electric field gradient around the electrodes. Figure 7(a) shows the electric field intensity inside the microchannel along the y-direction. As can be seen, the electric field maximizes at the edges of the electrodes and decreases with taking distance in the y-direction from the electrode. Considering "Fig. 7(b)", the electric field covers the entire width of the channel, where the DEP is the dominant force affecting the cells. It is notable that the simulation results are well compatible with the theoretical calculation.

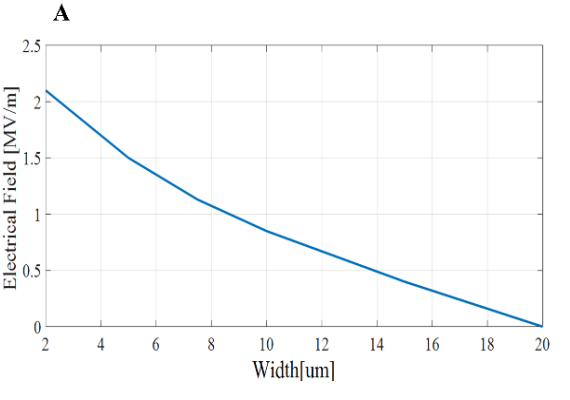

Fig. 7 (a): The electric field in y-direction.

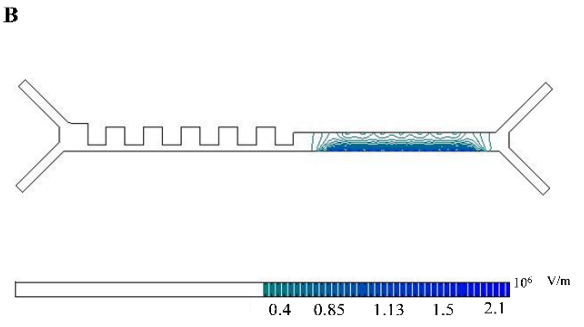

Fig. 7 (b): Electric field contour.

For the analysis of this part, through "Figs. 7 and 8", it can be concluded that the distribution of the electric potential and the gradient of the electric field are the same. As a result, the electric field is evenly distributed upper the electrodes and the cells experience a stable force.

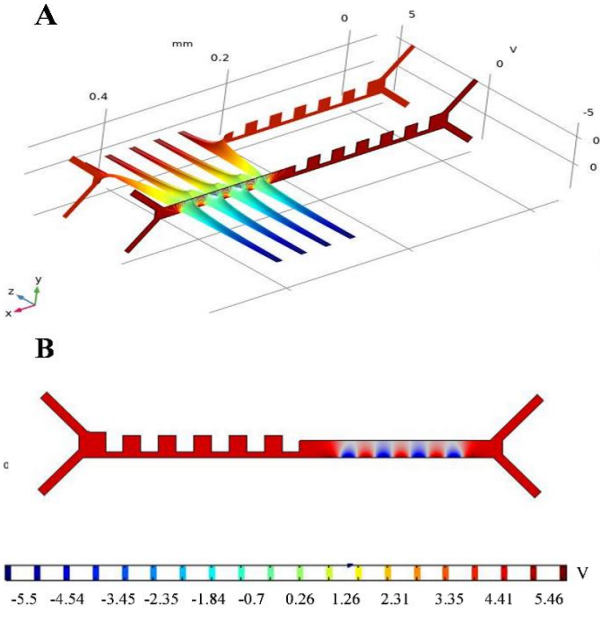

Fig. 8 (a): 3D electric potential contour, and (b): Electric potential contour.

It is notable that the force of dielectrophoresis is affected by the intensity of the electric field and the permeability and conductivity of the particles. So, the cancer cells are expected to be more affected by dielectrophoresis force as they have larger permeability and conductivity than WBCs. Figure 9 shows the magnitude of dielectrophoresis force versus different field intensities for both cancer cells and white blood ones.

Due to the less permeability and conductivity of WBCs compare to CTCs, dielectrophoresis phenomenon affects them less against the electric field application. The difference between the dielectrophoresis force effects on each particle becomes more significant as the electric field intensity increases.

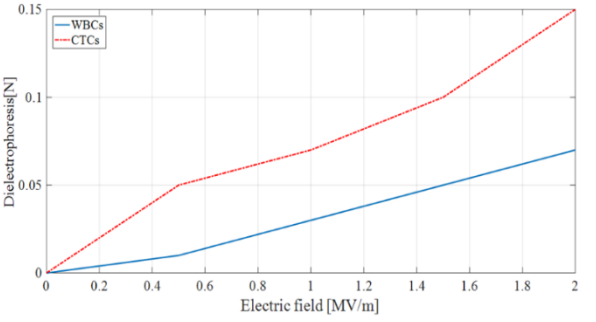

Fig. 9 Dielectrophoresis force for WBC and CTC as a function of electric field.

3.2. Fluid Velocity

The wall-induced lift force is created in the square section using a structure which expands and contracts, periodically. The fluid enters the channel at the velocity of 12um/s, then it enters the mixed part, where both sharp increment and decrement in its speed is observed. The velocity profile is parabolic, varying from zero velocity near the channel walls to the maximum value at the channel centre. Figure 10(a) shows the velocity of the fluid in different parts of the structure. The simulations demonstrate that the fluid movement inside the microchannel is uniform. Figure 10(b) shows that the flow profile is extended into each chamber as deep as 10um. However, a profundity of more than 10um empty volume shows where the flow velocity is zero.

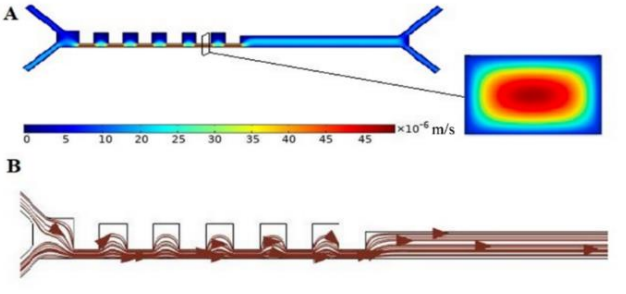

Fig. 10 (a): Fluid velocity contour at different parts of the structure, and (b): Fluid motion profile.

The drag force is depended on the velocity of the fluid. Increment of this force causes stress on the particles inside the square structure. The diagram of "Fig. 11" demonstrates the value of drag force inside the microchannel along the x-direction. In the region of the square structures, drag force is the dominant force affecting cells which is due to drastic changes in fluid velocity.

As shown in "Fig. 11", the highest fluid velocity rate inside the square structures is created in the parts where the channel is constricted. Therefore, in this section, the

most drag force is applied to the particles due to a sharp increment in velocity value. Consequently, in the parts where the channel is expanded, the velocity of the fluid decreases and fewer particles are affected.

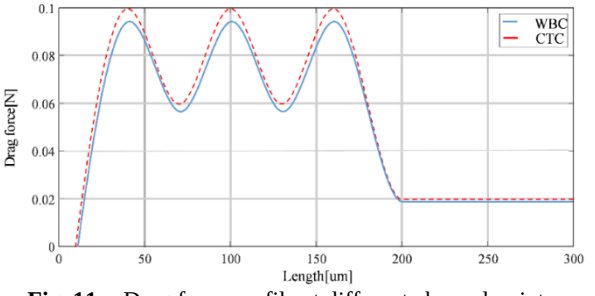

Fig. 11 Drag force profile at different channel points.

3.3. Particle Trajectory

As mentioned earlier, MCF-7 cells and WBCs overlap in size and are difficult to be separated. As shown in "Fig. 12", using a contractile and expanding channel, the wall-induced lift force is formed so the particles are first affected by this force and then by dielectrophoresis to perform a perfect particle separation. The proposed design which combines both wall-induced lift and dielectrophoresis forces, would achieve the separation efficiency of 100%. The particle trajectory is validated using the proposed dielectrophoresis approach with the experimental results presented by [16]

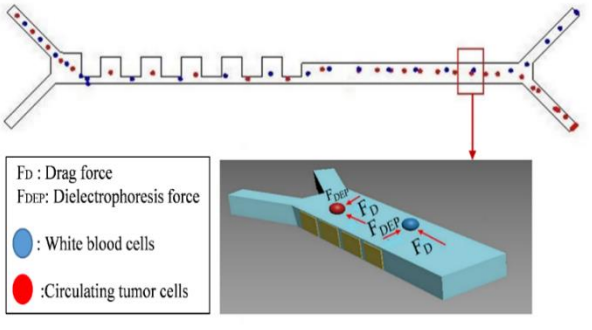

Fig. 12 Particle trajectories within the micro-channel.

Considering voltage application to the electrodes, the optimum separation performance of the structure is obtained in the voltage range of 5<V<7, which is 100% for the cancer cells and 99% for WBCs. Figure 13(a) demonstrates the efficiency versus the applied voltage, where at the voltages less than 5 V, the particles are not separated well and for the voltages above 7 V, the electric field increases too much and particles tends to stick to the electrodes. In addition, considering "Fig. 13(b)", increasing the fluid velocity more than 15um/s causes obstruction inside the microchannel. While for the velocities less than 15um/s, the particles do not reach the end of channel and would stick to the electrodes.

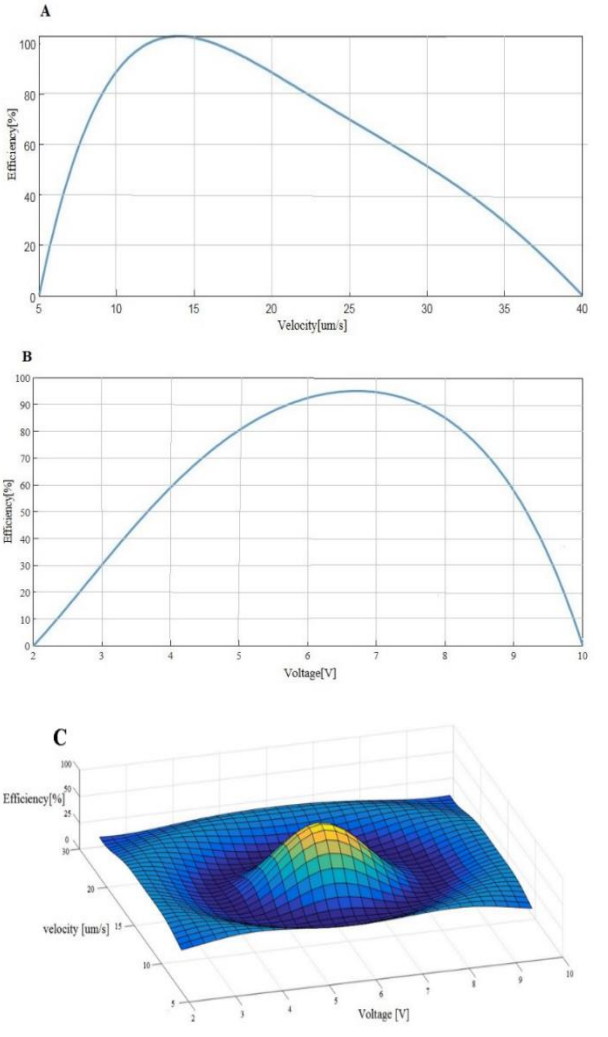

Fig. 13 Efficiency in terms of: (a): the applied voltage, (b): the fluid velocity, and (c): 3D efficiency of velocity and applied voltage.

Figure 14 illustrates a better description of the voltage value on the separation process of WBCs and CTCs.

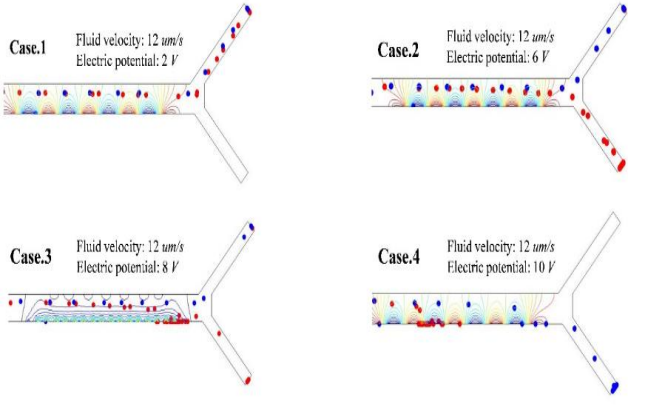

Fig. 14 Separation trajectories for different applied voltages.

Considering the first case with the applied voltage of 2V, the electric field created around the electrodes and the DEP force are not strong enough to perform the separation properly. In the second case, the applied voltage is increased to 6V and as is expected tends to a DEP force which separates the cells with the efficiency of 100%. Considering case 3, the electric field around the electrodes has its maximum intensity. As a result, the created DEP force causes the CTCs to be absorbed to the electrodes. The efficiency of this case is lower than 10%. For the last case, both CTCs and WBCs are absorbed to the electrodes and the efficiency of their separation is near zero.

In order to have a comparison between current investigation and previous studies, voltage, efficiency and channel width values are mentioned in "Table 3". As is obvious, in addition to the efficiency of 100%, not only the channel width, but also the applied voltage is reduced compared to other structures with the same yield.

Table 3 Comparison of the structures

Structure	Velocity [μm/s]	Channel width [μm]	Voltage [V]	Type of voltage	Efficiency
Han (2008)	-	25	5	Dc	87%
Park (2011)	13	30	10	Dc	98%
Dash (2016)	5	1000	200	Ac	99%
Kiel (2018)	-	1000	150	Ac	100%
Zhang (2020)	20	25	5	Dc	99%
This research	12	20	6	Dc	100%

4 CONCLUSION

In this paper, the plan of CTCs isolation from WBCs is investigated using both dielectrophoresis and wall-induced lift forces in a novel micro structure. Our proposed microfluidic design provides not only a simpler structure than the previous ones, but also its required applied voltage and fluid velocity are reduced. With the label-free separation efficiency of 100%, the maximum applied voltage to the electrodes has been reduced to 6V so as not to damage the blood cells and to provide a faster separation process. Considering the features of the proposed structure in this research, it can be used in medical and clinical processes as a laboratory chip.

REFERENCES

[1] Reguera, J., et al., Anisotropic Metal Nanoparticles for Surface Enhanced Raman Scattering, Chemical Society Reviews, Vol. 46, No. 13, 2017, pp. 3866-3885.

[2] Anbari, A., et al., Microfluidic Model Porous Media: Fabrication and Applications., Small, Vol. 14, No. 18, 2018, pp. 1703575.

[3] sonnenberg, a., et al., Dielectrophoretic Isolation and Detection of Cancer-Related Circulating Cell-Free DNA Biomarkers from Blood and Plasma, Electrophoresis, Vol. 35, No. 12-13, 2014, pp. 1828-1836.

[4] Tae-Hyeong K., et al., FAST: Size-Selective, Clog-Free Isolation of Rare Cancer Cells from Whole Blood at A Liquid–Liquid Interface, Analytical Chemistry, Vol. 89, No. 2, 2016, pp. 1155-1162.

[5] Qin X., et al., Size and Deformability-Based Separation of Circulating Tumor Cells from Castrate Resistant Prostate Cancer Patients Using Resettable Cell Traps, Lab on a Chip, Vol. 15, No. 10, 2015, pp. 2278-2286.

[6] Medema, J. P., Cancer Stem Cells: The Challenges Ahead, Nature cell biology, Vol. 15, No. 4, 2013, pp. 338-344.

[7] Ferlay, J. et al, Cancer Incidence and Mortality Worldwide: Sources, Methods and Major Patterns in Globocan 2012, International Journal of Cancer, Vol. 136, No. 5, 2015, pp. 359-386.

[8] Pommer, Matthew S., et al., Dielectrophoretic Separation of Platelets from Diluted Whole Blood in Microfluidic Channels, Electrophoresis, Vol. 29, No. 6, 2008, pp. 1213-1218.

[9] Han, K. H., Bruno Frazier, A., Lateral-Driven Continuous Dielectrophoretic Microseparators for Blood Cells Suspended in A Highly Conductive Medium, Lab on a Chip, Vol. 8, No. 7, 2008, pp. 1079-1086.

[10] Braschler, T., et al., Continuous Separation of Cells by Balanced Dielectrophoretic Forces at Multiple Frequencies, Lab on a Chip, Vol. 8, No. 2, 2008, pp. 280-286.

[11] Park, S., et al., Continuous Dielectrophoretic Bacterial Separation and Concentration from Physiological Media of High Conductivity, Lab on a Chip, Vol. 11, No. 17, 2011, pp. 2893-2900.

[12] Piacentini, N., et al, Separation of Platelets from Other Blood Cells in Continuous-Flow by Dielectrophoresis Field-Flow-Fractionation, Biomicrofluidics, Vol. 5, No. 3, 2011, pp. 034122.

[13] Patel, S., et al, Microfluidic Separation of Live and Dead Yeast Cells Using Reservoir-Based Dielectrophoresis, Biomicrofluidics, Vol. 6, No. 3, 2012, pp. 034102.

[14] Dash, S., et al., CFD Design of a Microfluidic Device for Continuous Dielectrophoretic Separation of Charged Gold Nanoparticles, Journal of the Taiwan Institute of Chemical Engineers, Vol. 58, 2016, pp. 39-48.

[15] Kale, A., Saurin P., and Xiangchun X., Three-dimensional reservoir-based dielectrophoresis (rDEP) for

Enhanced Particle Enrichment, Micromachines, Vol. 9, No. 3, 2018, pp. 123-128.

[16] Zhang X., et al., Numerical Simulation of Circulating Tumor Cell Separation in A Dielectrophoresis Based YY Shaped Microfluidic Device, Separation and Purification Technology, Vol. 255, 2020, pp. 117343.

[17] Kadaksham, J., Singh P., and Aubry. N., Manipulation of Particles Using Dielectrophoresis, Mechanics Research Communications, Vol. 33, No. 1, 2006, pp. 108-122.

[18] Bruus, H., Theoretical Microfluidics, Oxford: Oxford University Press, Vol. 18, 2008.

[19] Brenner, H., The Slow Motion of a Sphere Through a Viscous Fluid Towards a Plane Surface, Chemical Engineering Science, Vol. 16, No. 3-4, 1961, pp. 242-251.

[20] Nerguizian, V., et al., Analytical Solutions and Validation of Electric Field and Dielectrophoretic Force in A Bio-Microfluidic Channel, Electrophoresis, Vol. 33, No. 3, 2012, pp. 426-435.

[21] Tatsumi, K., et al., Analysis and Measurement of Dielectrophoretic Manipulation of Particles and Lymphocytes Using Rail-Type Electrodes, Medical Engineering & Physics, Vol. 38, No. 1, 2016, pp. 24-32.

[22] Egger, M., Donath E., Electrorotation Measurements of Diamide-Induced Platelet Activation Changes, Biophysical Journal, Vol. 68, No. 1, 1995, pp. 364-372.

[23] Yong Seok, C., Kyung Won, S., Sang Joon, L., Lateral and Cross-Lateral Focusing of Spherical Particles in A Square Microchannel, Lab on a Chip, Vol. 11, No. 3, 2011, pp. 460-465.

[24] Jones, T. B., Liquid Dielectrophoresis on The Microscale, Journal of Electrostatics, Vol. 51, 2001, pp. 290-299.

[25] Sungyoung C., Gwon Lee M., Je Kyun P., Microfluidic Parallel Circuit for Measurement of Hydraulic Resistance, Biomicrofluidics, Vol. 4, No. 3, 2010, pp. 034110.

[26] Myung Gwon L., Sungyoung C., Je Kyun P., Three-Dimensional Hydrodynamic Focusing with A Single Sheath Flow in A Single-Layer Microfluidic Device, Lab on a Chip, Vol. 9, No. 21, 2009, pp. 3155-3160.

[27] Myung Gwon L., et al., Inertial Blood Plasma Separation in A Contraction–Expansion Array Microchannel, Applied Physics Letters, Vol. 98, No. 25, 2011, pp. 253702.

[28] Myung Gwon, L., Sungyoung, and C., Je Kyun, P., Inertial Separation in A Contraction–Expansion Array Microchannel, Journal of Chromatography A, Vol. 1218, No. 27, 2011, pp. 4138-4143.

[29] Myung Gwon, L., et al., Label-Free Cancer Cell Separation from Human Whole Blood Using Inertial Microfluidics at Low Shear Stress, Analytical Chemistry, Vol. 85, No. 13, 2013, pp. 6213-6218.